AGU PUBLICATIONS

JGR

Journal of Geophysical Research: Space Physics

RESEARCH ARTICLE
10.1002/2013JA019587

Key Points:
- Localized ion acceleration occurs at quasi-parallel bow shock
- Shock accelerated ions are injected intothe magnetosheath
- Density and temperature structures are formed in the magnetosheath

Correspondence to:
N. Omidi,
omidi@solanasci.com

Citation:
Omidi, N., D. Sibeck, O. Gutynska, and K. J. Trattner (2014), Magnetosheath filamentary structures formed by ion acceleration at the quasi-parallel bow shock, *J. Geophys. Res. Space Physics*, *119*, 2593–2604, doi:10.1002/2013JA019587.

Received 31 OCT 2013
Accepted 26 FEB 2014
Accepted article online 4 MAR 2014
Published online 8 APR 2014

Magnetosheath filamentary structures formed by ion acceleration at the quasi-parallel bow shock

N. Omidi[1], D. Sibeck[2], O. Gutynska[2], and K. J. Trattner[3]

[1]Solana Scientific Inc., Solana Beach, California, USA, [2]NASA GSFC, Greenbelt, Maryland, USA, [3]LASP, University of Colorado, Boulder, Colorado, USA

Abstract Results from 2.5-D electromagnetic hybrid simulations show the formation of field-aligned, filamentary plasma structures in the magnetosheath. They begin at the quasi-parallel bow shock and extend far into the magnetosheath. These structures exhibit anticorrelated, spatial oscillations in plasma density and ion temperature. Closer to the bow shock, magnetic field variations associated with density and temperature oscillations may also be present. Magnetosheath filamentary structures (MFS) form primarily in the quasi-parallel sheath; however, they may extend to the quasi-perpendicular magnetosheath. They occur over a wide range of solar wind Alfvénic Mach numbers and interplanetary magnetic field directions. At lower Mach numbers with lower levels of magnetosheath turbulence, MFS remain highly coherent over large distances. At higher Mach numbers, magnetosheath turbulence decreases the level of coherence. Magnetosheath filamentary structures result from localized ion acceleration at the quasi-parallel bow shock and the injection of energetic ions into the magnetosheath. The localized nature of ion acceleration is tied to the generation of fast magnetosonic waves at and upstream of the quasi-parallel shock. The increased pressure in flux tubes containing the shock accelerated ions results in the depletion of the thermal plasma in these flux tubes and the enhancement of density in flux tubes void of energetic ions. This results in the observed anticorrelation between ion temperature and plasma density.

1. Introduction

The properties of the magnetosheath are determined by the conservation of mass, momentum, and energy across the bow shock (the Rankine–Hugoniot conditions) and collisionless dissipation processes upstream at and downstream of the bow shock. The most important solar wind parameters that impact the strength and the geometry of the bow shock are the Mach number, plasma beta (ratio of thermal to magnetic pressure), and the direction of the interplanetary magnetic field (IMF). The direction of the upstream magnetic field determines the regions of the bow shock corresponding to the quasi-parallel and quasi-perpendicular geometries, where shock dissipation processes are considerably different. In the quasi-perpendicular geometry, shock dissipation results in ions downstream from the bow shock having temperatures perpendicular to the magnetic field larger than parallel [e.g., *Leroy et al.*, 1982; *Sckopke et al.,* 1983, 1990]. The presence of this anisotropy results in the generation of ion cyclotron and mirror mode waves in the magnetosheath with the former propagating primarily along the magnetic field and latter simply being carried by the magnetosheath flow, because they have zero phase and group velocities [e.g., *Luhmann et al.*, 1986; *Lacombe et al.*, 1992; *Belmont et al.*, 1992; *Gary*, 1992; *Gary et al.*, 1993; *McKean et al.*, 1992, 1994; *Fazakerley and Southwood*, 1994; *Anderson et al.*, 1994; *Omidi et al.*, 1994; *Lacombe and Belmont*, 1995; *Lucek et al.,* 1999, 2001; *Gĕnot et al.*, 2009].

In the quasi-parallel regime, ion reflection and leakage at the shock result in the presence of a variety of backstreaming foreshock ion beam populations [*Asbridge et al.*, 1968; *Greenstadt et al.*, 1968, 1980; *Gosling et al.*, 1978; *Paschmann et al.*, 1979; *Bonifazi et al.,* 1980a, 1980b]. The interaction of these ions with the solar wind generates a number of different ULF waves and nonlinear structures that get carried back by the solar wind and impact the magnetosheath [e.g., *Fairfield*, 1969; *Hoppe et al.*, 1981; *Russell and Hoppe,* 1983; *Gary et al.*, 1984; *Le and Russell*, 1992; *Greenstadt et al.*, 1995; *Blanco-Cano and Schwartz*, 1995; *Lin*, 2003; *Omidi,* 2007; *Blanco-Cano et al.*, 2009, 2011; *Kajdič et al.,* 2010, 2011; *Omidi et al.*, 2013; *Zhang et al.*, 2013]. The presence of tangential or rotational discontinuities in the solar wind and their interaction with the foreshock or bow shock result in the formation of structures such as foreshock bubbles or hot flow anomalies with significant effects on the magnetosheath [e.g., *Schwartz et al.*, 1988, 2000; *Schwartz*, 1995; *Thomsen et al.,* 1986, 1988, 1993; *Paschmann et al.*, 1988; *Thomas et al.*, 1991; *Sibeck et al.,* 1998, 1999, 2000; *Lin*, 1997, 2002;

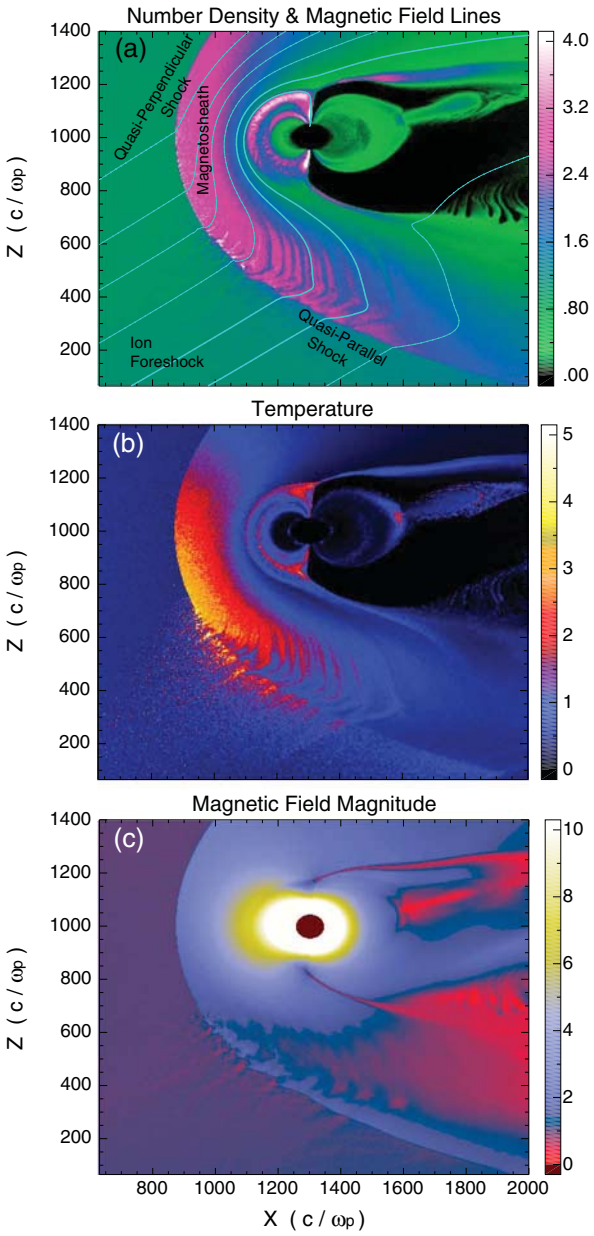

Figure 1. Results from a run with Alfvén Mach number of 3 and IMF cone angle of 35°. (a) The plasma density normalized to solar wind value and magnetic field lines. (b) The ion temperature normalized to its solar wind value. (c) The total magnetic field strength normalized to IMF value with the maximum value artificially set at 10 to make the magnetosheath more visible.

Lucek et al., 2004; *Omidi and Sibeck*, 2007; *Facsko et al.*, 2008; *Eastwood et al.*, 2008; *Jacobsen et al.*, 2009; *Omidi et al.*, 2010; *Turner et al.*, 2013]. Solar wind transients and their interactions with the bow shock can also result in the generation of waves and density pulses in the magnetosheath [e.g., *Sibeck and Gosling*, 1996; *Němeček et al.*, 1998; *Seon et al.*, 1999; *Zastenker et al.*, 2002; *Savin et al.*, 2008; *Amata et al.*, 2011; *Turner et al.*, 2011; *Karlsson et al.*, 2012].

In this paper, we use the results from 2.5-D global hybrid simulations to demonstrate for the first time the formation of field-aligned density and temperature enhancements that we call magnetosheath filamentary structures (MFS). These are large structures that begin at the quasi-parallel bow shock and extend well into the magnetosheath as far as the magnetopause. MFS form over a wide range of solar wind Mach numbers and IMF cone angles (defined as the angle between IMF and solar wind velocity). We show that their formation is tied to localized ion acceleration processes at the quasi-parallel bow shock and is a direct result of ion dissipation processes at the bow shock. In the following section, we briefly describe the hybrid simulation model and show the results that illustrate the formation of MFS under a variety of Mach numbers and IMF cone angles. Section 3 provides a summary and conclusions.

2. Simulation Results

We use 2.5-D (3-D in velocity and fields and 2-D in space) electromagnetic hybrid (kinetic ions and fluid electrons) simulations to examine the formation of MFS. This model has been used extensively in the past and has resulted in a number of predictions subsequently observed by spacecraft [e.g., *Omidi et al.*, 2004, 2005, 2006, 2009a, 2009b, 2010, 2013; *Omidi and Sibeck*, 2007; *Blanco-Cano et al.*, 2006a, 2006b, 2009, 2011; *Sibeck et al.*, 2008; *Turner et al.*, 2013; *Zhang et al.*, 2013]. The four equations that are solved include Ampere's law without the displacement current (called the Darwin approximation) so that high-frequency light waves are eliminated. The second equation is Faraday's law, while the third is the electron momentum equation with electron mass equal to zero. This leads to the generalized Ohm's law that includes the Hall term and electron pressure gradients. Electrons are assumed to behave adiabatically. The model has a magnetic dipole inside a conducting sphere whose surface represents the ionospheric boundary. The simulation box lies in the noon-midnight meridian plane with x along the solar wind velocity (Sun-Earth line) and the magnetic dipole moment in the z direction. The simulation domain covers 2000 ion skin depths c/ω_p (where c is

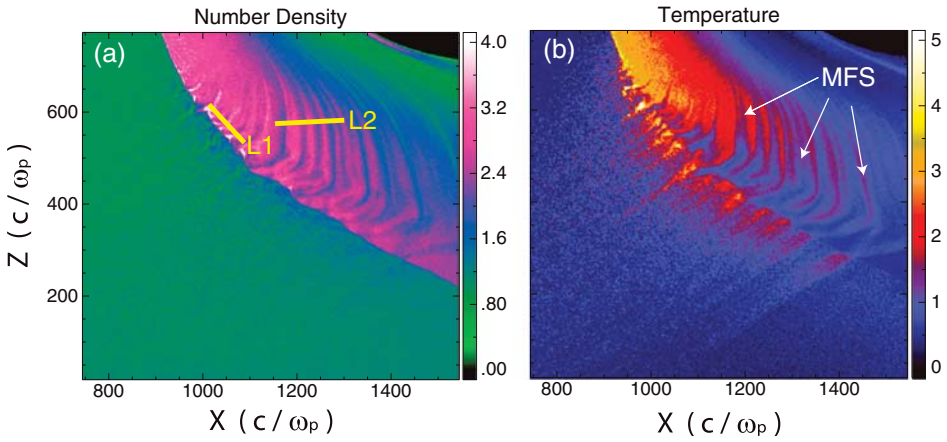

Figure 2. (a) The plasma density zoomed near the quasi-parallel bow shock and magnetosheath. (b) The ion temperature in the same area as in Figure 2a. Figures 2a and 2b both show density and temperature enhancements associated with MFS.

the speed of light and ω_p is the ion plasma frequency) in the x and z directions with a cell size of 1 ion skin depth (see *Omidi and Sibeck* [2007] for the discussion on the choice of cell size in global hybrid simulations). Solar wind plasma is injected from the left boundary and allowed to leave the system through the remaining boundaries. The results discussed here correspond to solar wind conditions with Alfvén Mach number between 3 and 11 and IMF cone angles (with respect to x axis) of 35° and 5°.

Figure 1 shows the output from a run with an Alfvén Mach number of 3 and IMF cone angle of 35° zoomed mostly on the quasi-parallel (southern) portion of the bow shock. Figure 1a shows the density normalized to its solar wind value and magnetic field lines, Figure 1b shows the ion temperature normalized to the corresponding solar wind value, and Figure 1c shows the total magnetic field strength normalized to the IMF value. In Figure 1c, the scale is set to a maximum of 10 in order to make the bow shock and magnetosheath visible. The density and temperature panels show the presence of field-aligned, filamentary structures in the quasi-parallel magnetosheath. On the other hand, there are no signs of filamentary magnetic field structures within the southern magnetosheath behind the quasi-parallel bow shock where, except near the shock, magnetic field strengths are comparable to those in the solar wind as expected from the Rankine–Hugoniot conditions.

To view the magnetosheath filamentary structures in more detail, Figure 2 shows the density and temperature from the same run as in Figure 1 in the quasi-parallel portion of the sheath. It is evident in Figure 2b that the filamentary structures in the magnetosheath are connected to the regions of localized high-energy ions upstream of the shock. Figure 3 shows the variations of the magnetic field, ion temperature, and density along the lines L1 and L2 (length of ~100 c/ω_p) in Figure 2a. Figures 3a–3c correspond to L1 and show an evidence of oscillations in the magnetic field, temperature, and density. It is evident that the wavelength of the oscillations in temperature and density is shorter than that associated with the magnetic field. The latter is associated with waves in the magnetosheath not connected to MFS. In addition, the fluctuations in density and temperature are anticorrelated. Figures 3d–3f correspond to line L2 and again show anticorrelated fluctuations in density and temperature with no corresponding variations in the magnetic field. The results in Figure 3 indicate that the magnetosheath filamentary structures are primarily a nonmagnetic phenomenon; however, as we show below near the bow shock, these structures may be associated with magnetic field oscillations.

Figures 4a through 4f show the ion temperature at 6 times $\Omega t = 212.5$, 275, 337.5, 400, 462.5, and 500 (where Ω is the proton cyclotron frequency) and illustrate the evolution of the magnetosheath filamentary structures. MFS initially form at lower latitudes closer to the nose of the bow shock and subsequently get carried away from the nose as they continue to evolve. As a result, the number of filamentary structures increases with time as new ones are generated near the nose and then convected antisunward to higher (southern) latitudes. Figure 5 shows the transverse or dawn/dusk (B_y) component of the magnetic field at the same times as in Figure 4 and demonstrates the presence of waves upstream of the bow shock at all times shown. These are circularly polarized waves propagating along the magnetic field and are generated by the backstreaming ions seen in Figure 4 (see *Blanco-Cano et al.* [2006a, 2006b, 2009, 2011], *Omidi*

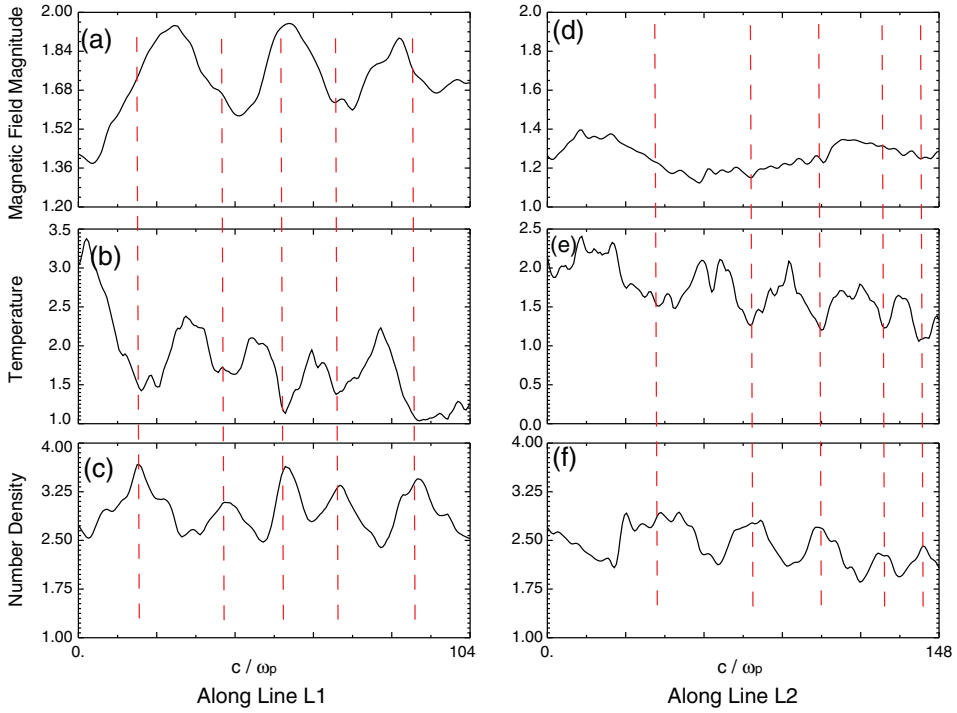

Figure 3. (a–c) The variations of magnetic field strength, ion temperature, and density along line labeled L1 in Figure 2a. (d–f) The variations of magnetic field strength, ion temperature, and density along line labeled L2 in Figure 2a. Note the anticorrelated oscillations in density and temperature associated with MFS.

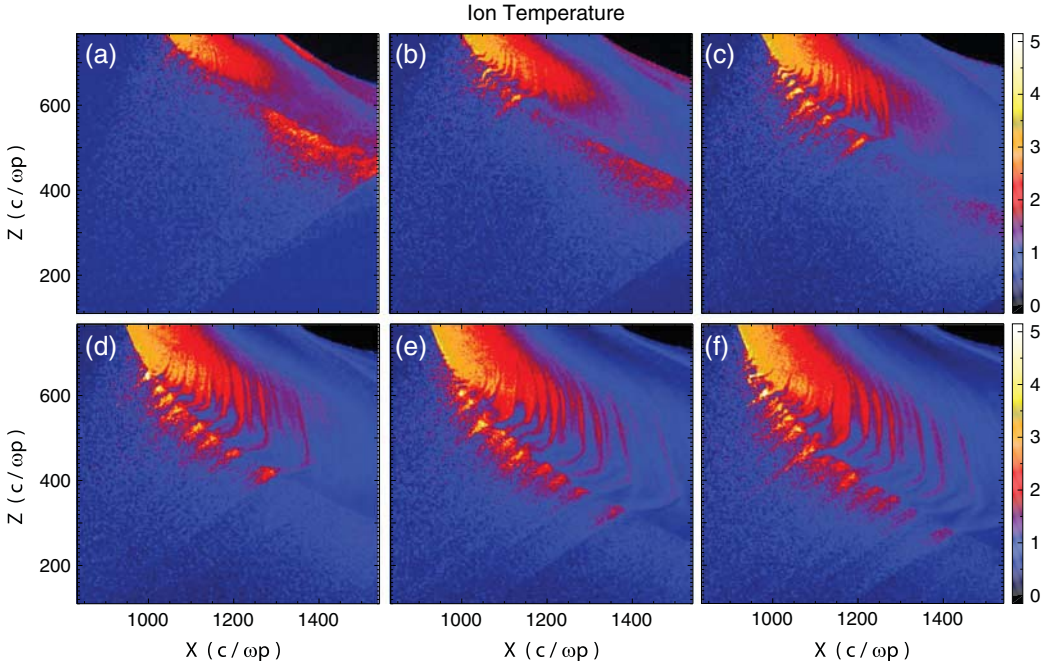

Figure 4. (a–f) The ion temperature in the foreshock and quasi-parallel magnetosheath at different times illustrating the formation and evolution of MFS.

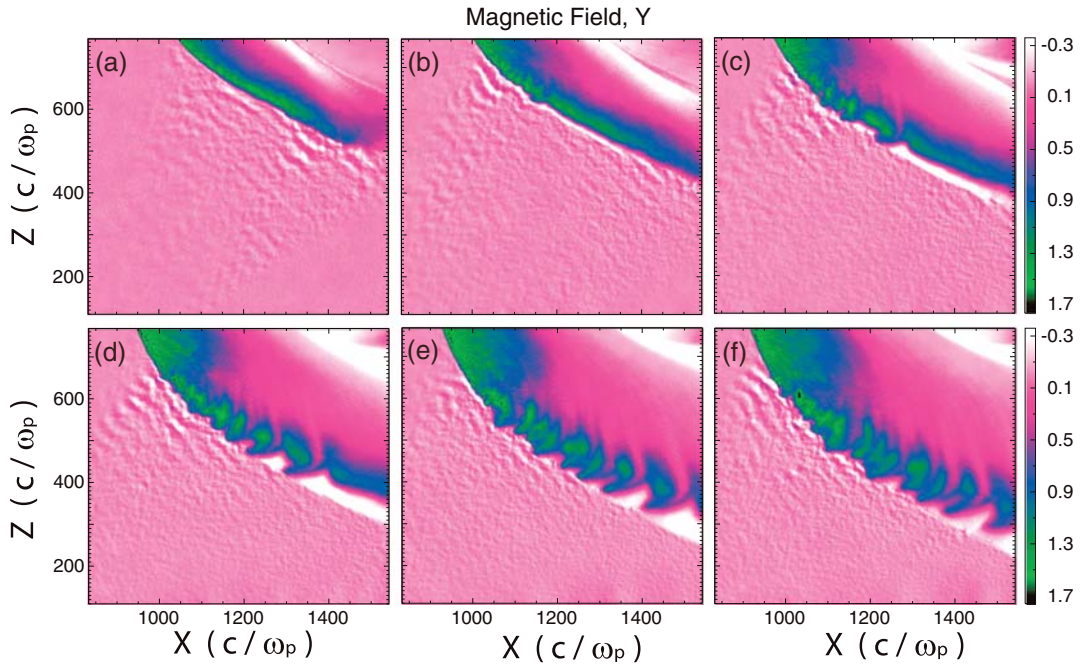

Figure 5. (a–b) The transverse component of the magnetic field at the same time as those in Figure 4. They show the presence of waves in the foreshock at all times and also the generation of oscillations in the magnetosheath near the quasi-parallel bow shock.

[2007], and *Omidi et al.* [2005] for detailed analysis and discussion of upstream waves in global hybrid simulations). They have wave vectors that point toward the Sun, but because their group velocity is smaller than the solar wind speed, they are convected back toward the shock. Figure 5 also shows the presence of waves in the magnetosheath near the bow shock that, similar to MFS, originate close to the nose of the bow shock and travel to higher latitudes with time. The connection between MFS and these waves will be discussed shortly.

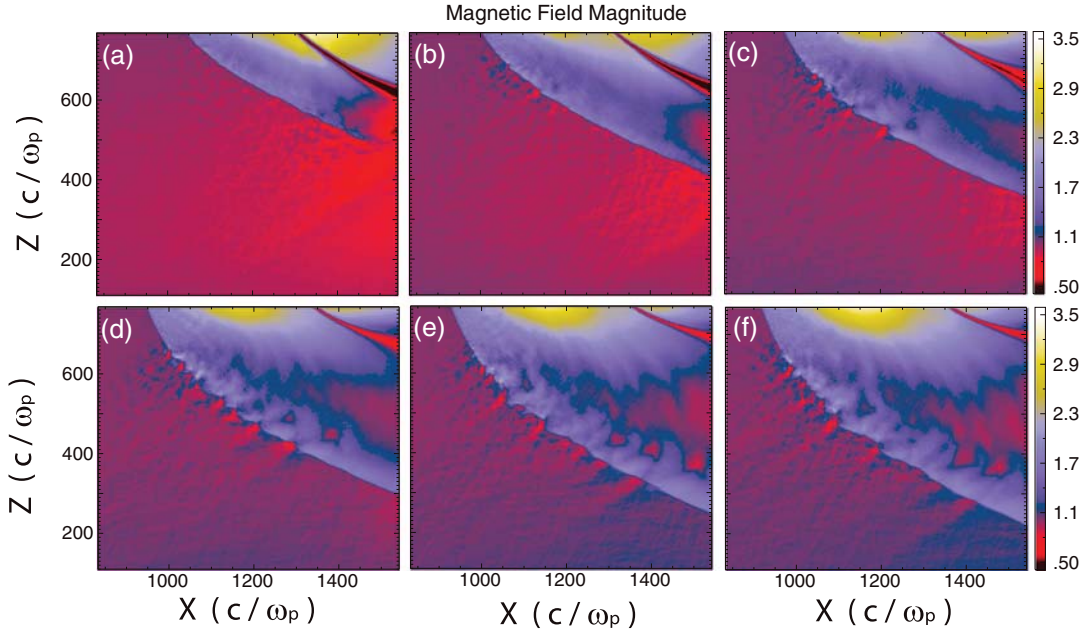

Figure 6. (a–b) The total magnetic field at the same time as those in Figures 4 and 5. They show the generation of fast magnetosonic waves at large wave angles with respect to magnetic field.

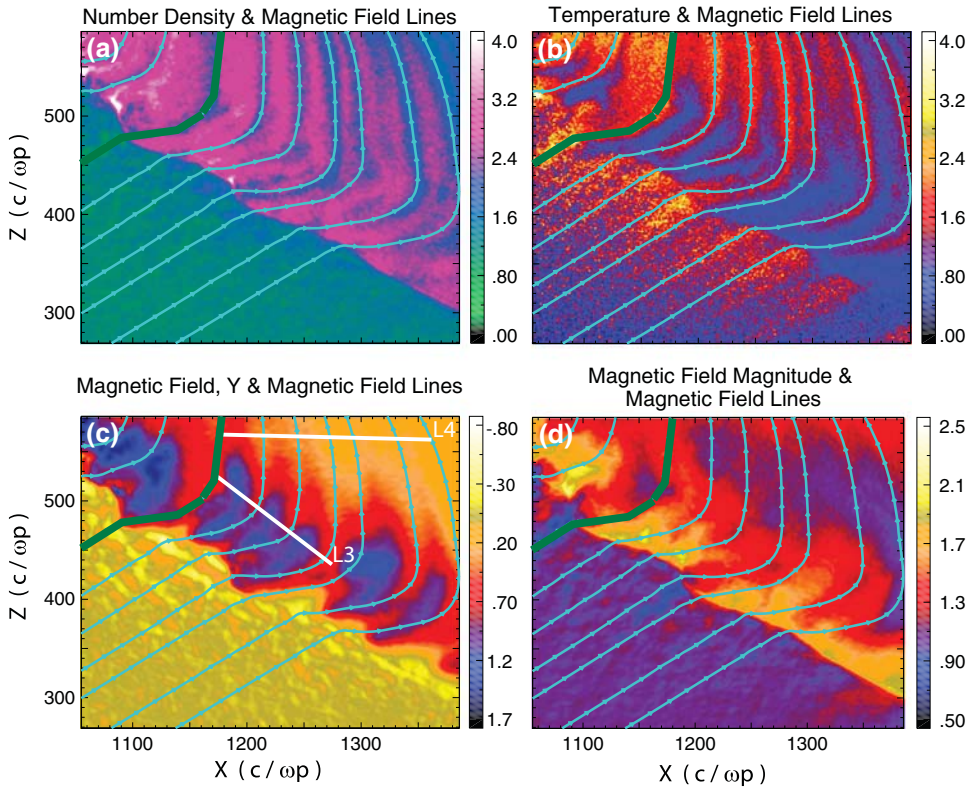

Figure 7. (a–d) The density, ion temperature, transverse magnetic field, and total magnetic field zoomed near the quasi-parallel bow shock and sheath. Also shown are the same set of magnetic field lines in each panel.

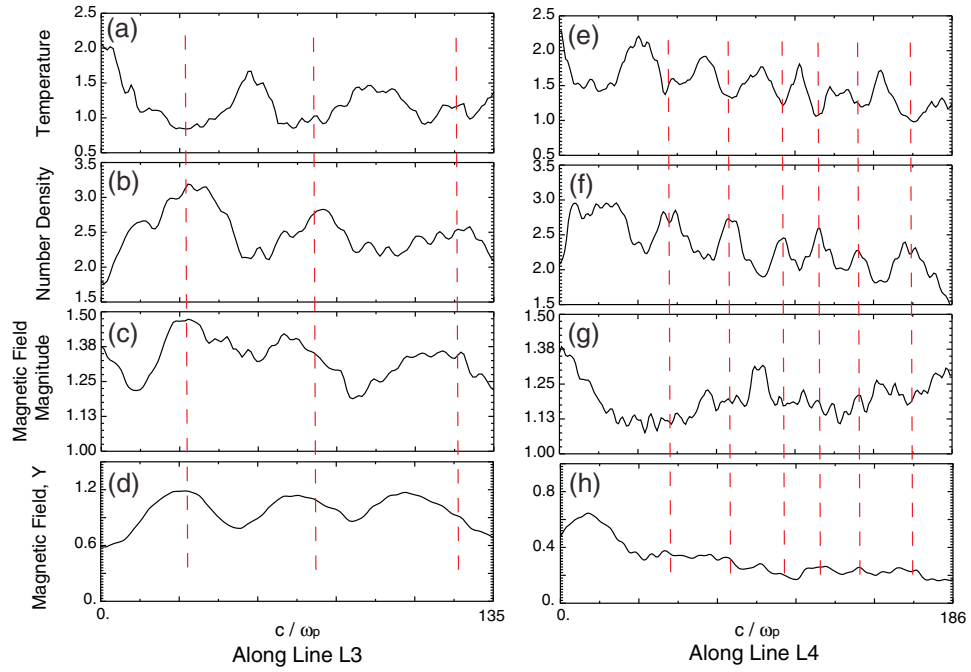

Figure 8. (a–d) The variations of ion temperature, density, magnetic field strength, and transverse magnetic field along line labeled L3 in Figure 7c. (e–h) The variations of ion temperature, density, magnetic field strength, and transverse magnetic field along line labeled L4 in Figure 7c.

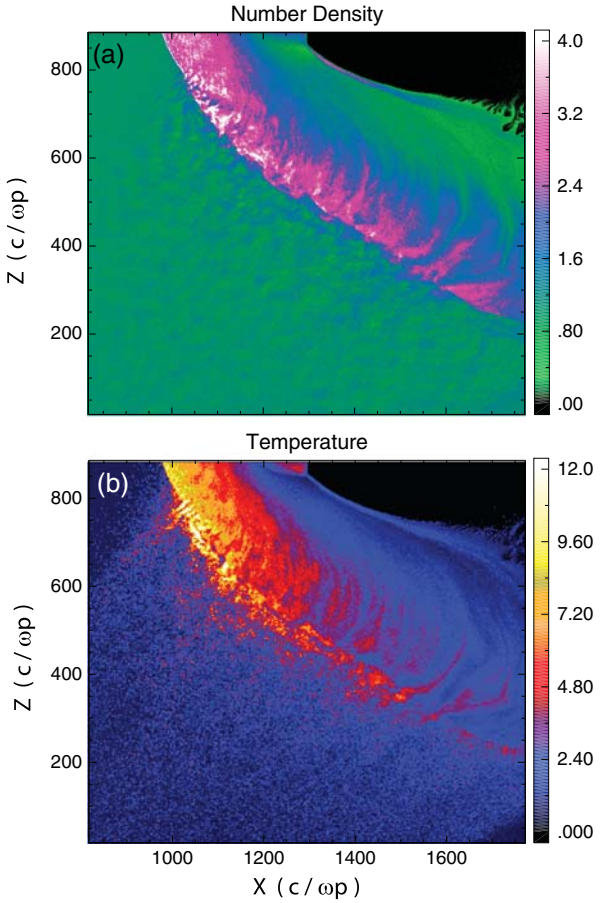

Figure 9. (a and b) The plasma density and ion temperature zoomed near the quasi-parallel bow shock from a run with Alfvén Mach number of 5 and IMF cone angle of 35°.

Figures 6a through 6f show the total magnetic field strength at the same times as in Figures 4 and 5. Early in the run (Figure 6a), no fluctuations in the total magnetic field are present in the foreshock, consistent with the transverse nature of the parallel propagating waves in that region. At later times, Figure 6 shows the appearance of magnetic fluctuations near and upstream of the bow shock that originate at lower latitudes and appear at higher latitudes with time. These are fast magnetosonic waves that propagate at large angles to the upstream magnetic field. They were first discussed by *Omidi* [2007] and *Blanco-Cano et al.* [2011], who showed that the backstreaming ions in the foreshock not only generate the transverse, parallel waves but also highly oblique fast magnetosonic waves. The growth rate of these waves increases with the energy of the backstreaming ions. So in the initial formation of the shock in the simulation, the energy of the backstreaming ions is not high enough for appreciable growth of magnetosonic waves, and only parallel propagating waves are excited (Figure 6a). However, as higher-energy ions originating from the nose region of the magnetosheath leak into the upstream region, fast magnetosonic waves are also excited (Figures 6b–6f). These waves are convected into the magnetosheath and result in the oscillations in B_y seen in Figure 5.

Magnetosonic waves are responsible for the localized acceleration of the ions at the bow shock and the formation of MFS. Figure 7 illustrates more details on the structure of MFS and shows density, temperature, B_y, and total magnetic field zoomed on the quasi-parallel bow shock and magnetosheath. Also plotted are magnetic field lines in the four panels so that we can focus on individual field lines and examine the details of the MFS structure. For example, the examination of the third magnetic field line (thicker and green color) from the upper left corner in Figure 7a shows that it falls in a region of low density in the magnetosheath. Figure 7b shows that the same field line falls in a region of high ion temperature in the magnetosheath consistent with the anticorrelation of density and temperature described earlier. It is also evident that this field line connects to a region of higher ion temperature in the foreshock and at the bow shock. As can be seen in Figure 7d, this region of higher temperature corresponds to lower magnetic field strengths and is bounded by higher magnetic fields associated with the fast magnetosonic waves. Similar patterns are associated with the other field lines depicted in Figure 7, indicating that the magnetosonic waves cause localized ion temperature enhancements in the foreshock. The energized ions follow magnetic field lines into the magnetosheath. Here enhanced pressures associated with the energetic ions cause expansions that diminish plasma densities on these field lines. By contrast, neighboring regions with fewer or no energetic ions are compressed, resulting in density enhancements. This leads to the consistent anticorrelation seen between density and temperature changes associated with MFS.

The examination of Figures 7c and 7d shows that the fluctuations in B_y and total magnetic field are present in the sheath near the bow shock. The regions of enhanced B_y and field strength coincide with each other and also line up with peaks in the magnetic field strength upstream of the shock. This indicates that the magnetosheath oscillations result from the convection of upstream magnetosonic waves into the

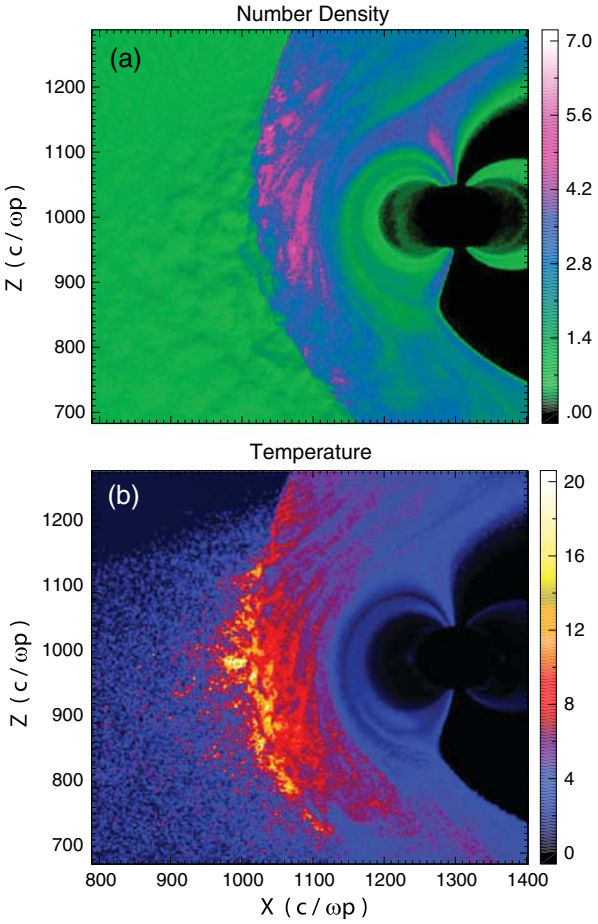

Figure 10. (a and b) The plasma density and ion temperature from a run with Alfvén Mach number of 5 and IMF cone angle of 5°.

downstream. Since the structure of the MFS and the spacing between the filaments are controlled by the upstream magnetosonic waves, one would expect some form of correlation between the oscillations in B_y and total field and MFS near the bow shock. To examine this possibility, Figures 8a–8d show ion temperature, density, magnetic field strength, and B_y along the line L3 shown in Figure 7. It is evident that density and magnetic field are correlated with each other and anticorrelated with temperature. The correlation between density and magnetic field is consistent with the signatures expected for a fast magnetosonic mode. Figures 8e–8h show the variations of the magnetosheath plasma and magnetic field along the line L4 in Figure 7 and demonstrate that further away from the bow shock, MFS shows no correlated changes in magnetic field. Thus, given the connection between the upstream fast magnetosonic waves and MFS and the convection of the former into the magnetosheath, we find oscillations in the magnetic field that correlate with MFS near the bow shock. However, further into the magnetosheath, the MFS has no magnetic component and consists solely of density and temperature oscillations.

The results of hybrid simulations show that MFS form over a wide range of Mach numbers and IMF cone angles. Figures 9a and 9b show the density and temperature from a run with IMF cone angle of 35° and solar wind Alfvén Mach number of 5. The formation of MFS in the quasi-parallel magnetosheath is evident and demonstrates that it is not only associated with low Mach number bow shock. There is however a change in the quasi-parallel bow shock at higher Mach numbers in that spontaneous hot flow anomalies (SHFAs) are formed as part of the shock dissipation process [*Omidi et al.*, 2013; *Zhang et al.*, 2013]. SHFAs are cavities containing low solar wind densities and magnetic field strengths and enhanced fluxes of high-energy particles with rims exhibiting enhanced densities and magnetic field strengths. They form as a result of the convection of foreshock cavitons into the quasi-parallel bow shock. The formation of foreshock cavitons was predicted by hybrid simulations [*Lin,* 2003; *Lin and Wang*, 2005; *Omidi,* 2007], and they were discovered in spacecraft data by *Blanco-Cano et al.* [2009, 2011] and *Kajdič et al.* [2010, 2011]. As demonstrated by *Omidi* [2007], foreshock cavitons result from the simultaneous generation of parallel propagating electromagnetic waves and oblique fast magnetosonic waves by the backstreaming ions and their highly coupled nonlinear evolution. The formation of SHFAs at the bow shock also results in localized regions of high-energy ions that are injected into the magnetosheath along the field line resulting in the formation of MFS. We note that at both low and high Mach numbers, the role of fast magnetosonic waves in forming localized regions of higher ion temperature at the bow shock is similar.

The results presented so far correspond to an IMF cone angle of 35° with MFS forming mostly away from the dayside magnetopause and carried away with the magnetosheath flow. At lower IMF cone angles, the MFS forms upstream of the dayside magnetopause and stays more stationary due to the low flow velocity of the magnetosheath in that region. Figures 10a and 10b show the density and ion temperature from a run with an Alfvén Mach number of 5 and an IMF cone angle of 5°. The formation of MFS in the low-latitude dayside

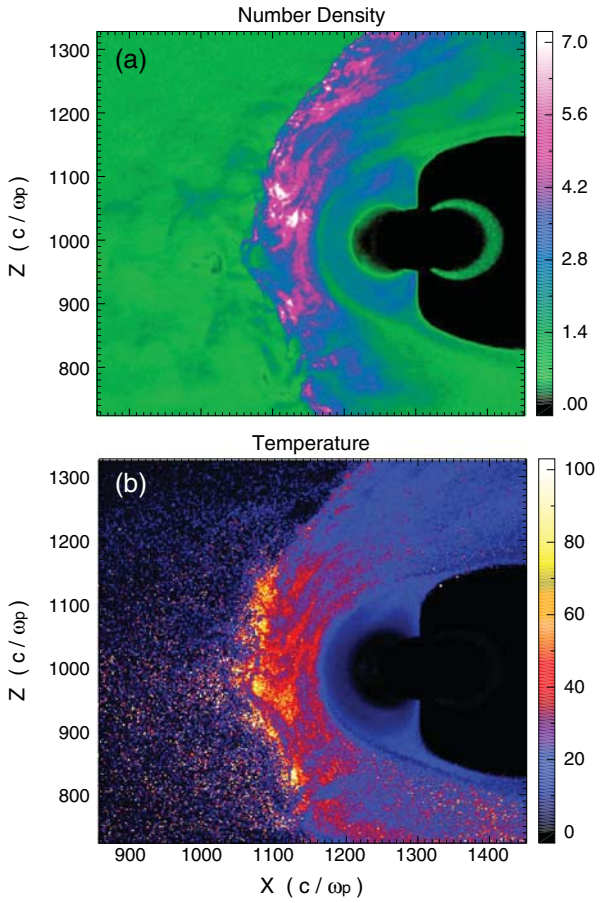

Figure 11. (a and b) The plasma density and ion temperature from a run with Alfvén Mach number of 11 and IMF cone angle of 5°.

magnetosheath is evident in both the density and temperature plots. In contrast to the case for higher IMF cone angles, where the filaments lie nearly parallel to vector pointing radially away from Earth and move poleward, the density and temperature perturbations associated with the MFS in Figure 10 lie nearly perpendicular to the radial direction. Figure 11 is similar to Figure 10 except that it corresponds to a run with a higher Alfvénic Mach number of 11. The MFS structure in Figure 11 is similar to that in Figure 10, because the IMF cone angle is the same in both runs. Comparing Figure 10a and Figure 11a demonstrates that while MFS forms in both runs, the magnetosheath in Figure 11 has a more turbulent structure due to the higher solar wind Mach number. The enhanced turbulence causes the magnetic field lines that comprise the MFS to bend and twist into more complicated forms.

3. Summary and Conclusions

Using global, electromagnetic hybrid simulations, we show the formation of magnetosheath filamentary structures: namely, field-aligned density and temperature structures in the magnetosheath. They begin at the quasi-parallel bow shock and extend well into the quasi-parallel magnetosheath reaching as far as the magnetopause. When the IMF cone angle is small, MFS may extend into the quasi-perpendicular magnetosheath. The antisunward convection of MFS that are stationary in the plasma rest frame results in anticorrelated magnetosheath density and temperature fluctuations. The fluctuations are nearly stationary in the low flow speed subsolar magnetosheath but produce Doppler shifted frequencies in the higher-latitude magnetosheath, where flow speeds are greater. In general, MFS are not associated with magnetic field changes; however, near the bow shock, the presence of transmitted fast magnetosonic waves may show magnetic field oscillations that correlate well with MFS associated density and temperature variations. The convection of the parallel propagating waves in the upstream results in magnetic field variations at and downstream of the shock that would not correlate with density and temperature oscillations associated with MFS.

Magnetosheath filamentary structures form over a wide range of solar wind Mach numbers and IMF cone angles. In all cases, their formation is tied to the presence of localized regions of enhanced ion temperature at and upstream of the quasi-parallel bow shock. Upon injection of these energetic ions into the magnetosheath, they follow the field line and form a temperature filamentary structure whose enhanced pressure reduces the plasma density in the same flux tube but increases it in the surrounding flux tubes. This accounts for the observed anticorrelations between density and temperature fluctuations associated with MFS. The formation of localized regions of enhanced ion temperature at and upstream of the bow shock is connected to the generation of fast magnetosonic waves propagating at large angles to the upstream magnetic field. At low Mach numbers, these waves result in local acceleration of ions upstream of the bow shock through interaction with the parallel propagating, circularly polarized electromagnetic waves that are also generated by the back streaming ions. At higher Mach numbers, the nonlinear evolution of the fast and parallel propagating waves results in the

formation of foreshock cavitons, whose convection into the bow shock results in the generation of SHFAs and localized enhancements of temperature.

The scale length associated with MFS, namely, the distance between the filaments is primarily determined by the distance between the regions of high ion temperature at the quasi-parallel bow shock. This spacing is related to the wavelength of the fast magnetosonic waves and is ~30–60 ion skin depth, which corresponds to ~0.5–1 R_E. For magnetosheath velocities of 100–300 km/s, the expected frequency of the MFS oscillations would be in the range of 0.01–0.1 Hz assuming flow along the wave vector. In general, this assumption may not be true, and a determination of the local angle between the flow velocity and the direction of the wave vector may be needed in order to assess the Doppler frequency of MFS oscillations.

Acknowledgments
Work for this project was supported by NSF grants AGS-1007449, AGS-1103227, and 1102572.

Masaki Fujimoto thanks the reviewers for their assistance in evaluating this paper.

References

Amata, E., S. P. Savin, D. Ambrosino, Y. V. Bogdanova, M. F. Marcucci, S. Romanov, and A. Skalsky (2011), High kinetic energy density jets in the Earth's magnetosheath: A case study, *Planet. Space Sci.*, *59*, 482–494, doi:10.1016/j.pss.2010.07.021.

Anderson, B. J., S. A. Fuselier, S. P. Gary, and R. E. Denton (1994), Magnetic spectral signatures in the Earth's magnetosheath and plasma depletion layer, *J. Geophys. Res.*, *99*, 5877–5891.

Asbridge, J. R., S. J. Bame, and I. B. Strong (1968), Outward flow of protons from the earth's bow shock, *J. Geophys. Res.*, *73*, 5777–5782.

Belmont, G., D. Hubert, C. Lacombe, and F. Pantellini (1992), Mirror mode and other compressive ULF modes, Proceedings of the 26th ESLAB symposium, Killarney, Ireland, 16–19 June 1992, ESA SP-346, pp. 263.

Blanco-Cano, X., and S. J. Schwartz (1995), AMPTE-UKS observations of low frequency waves in the ion foreshock, in *Physics of Collisionless Shocks*, Advances in Space Research, vol. 15, edited by C. T. Russell, p. 97, Pergamon, Tarrytown, N. Y.

Blanco-Cano, X., N. Omidi, and C. T. Russell (2006a), Macro-Structure of Collisionless Bow Shocks: 2. Wave properties, *J. Geophys. Res.*, *111*, A10205, doi:10.1029/2005JA011421.

Blanco-Cano, X., N. Omidi, and C. T. Russell (2006b), ULF waves and their influence on bow shock and magnetosheath structures, *Adv. Space Res.*, *37*, 1522–1531, doi:10.1016/j.asr.2005.10.043.

Blanco-Cano, X., N. Omidi, and C. T. Russell (2009), Global hybrid simulations: Foreshock waves and cavitons under radial IMF geometry, *J. Geophys. Res.*, *114*, A01216, doi:10.1029/2008JA013406.

Blanco-Cano, X., P. Kajdič, N. Omidi, and C. T. Russell (2011), Foreshock cavitons for different interplanetary magnetic field geometries: Simulations and observations, *J. Geophys. Res.*, *116*, A09101, doi:10.1029/2010JA016413.

Bonifazi, C., A. Egidi, G. Moreno, and S. Orsini (1980a), Backstreaming ions outside the earth's bow shock and their interaction with the solar wind, *J. Geophys. Res.*, *85*, 3461–3472.

Bonifazi, C., G. Moreno, A. J. Lazarus, and J. D. Sullivan (1980b), Deceleration of the solar wind in the earth's foreshock region: ISEE 2 and IMP 8 observations, *J. Geophys. Res.*, *85*, 6031–6038.

Eastwood, J. P., et al. (2008), Themis observations of a hot flow anomaly: Solar wind, magnetosheath, and ground-based measurements, *Geophys. Res. Lett.*, *35*, L17S03, doi:10.1029/2008GL033475.

Facsko, G., K. Kecskemety, G. Erdos, M. Tatrallyay, P. W. Daly, and I. Dandouras (2008), A statistical study of hot ow anomalies using Cluster data, *Adv. Space Res.*, *41*(8), 1286, doi:10.1016/j.asr.2008.02.005.

Fairfield, D. H. (1969), Magnetic fields of the magnetosheath, *Rev. Geophys. Space Phys.*, *14*, 117–134.

Fazakerley, A. N., and D. J. Southwood (1994), Mirror instability in the magnetosheath, *Adv. Space Res.*, *14*, 65–68.

Gary, S. P. (1992), The mirror and ion cyclotron anisotropy instabilities, *J. Geophys. Res.*, *97*, 8519–8529.

Gary, S. P., C. W. Smith, M. A. Lee, M. L. Goldstein, and D. W. Forslund (1984), Electromagnetic ion beam instabilities, *Phys. Fluids*, *27*, 1852.

Gary, S. P., S. A. Fuselier, and B. J. Anderson (1993), Ion anisotropy instabilities in the magnetosheath, *J. Geophys. Res.*, *98*, 1481–1488.

Gĕnot, V., E. Budnik, P. Hellinger, T. Passot, G. Belmont, P. M. Trávníček, P.-L. Sulem, E. Lucek, and I. Dandouras (2009), Mirror structures above and below the linear instability threshold: Cluster observations, fluid model and hybrid simulations, *Ann. Geophys.*, *27*, 601–615.

Gosling, J. T., J. R. Asbridge, S. J. Bame, G. Paschmann, and N. Sckopke (1978), Observations of two distinct populations of bow shock ions in the upstream solar wind, *J. Geophys. Res.*, *5*, 957–960.

Greenstadt, E. W., I. M. Green, G. T. Inouye, A. J. Hundhausen, S. J. Bame, and I. B. Strong (1968), Strong, correlated magnetic field and plasma observations of the Earth's bow shock, *J. Geophys. Res.*, *73*, 51–60.

Greenstadt, E. W., C. T. Russell, and M. Hoppe (1980), Magnetic field orientation and suprathermal ion streams in the earth's foreshock, *J. Geophys. Res.*, *85*, 3473–3479.

Greenstadt, E. W., G. Le, and R. J. Strangeway (1995), ULF waves in the foreshock, in *Physics of Collisionless Shocks*, Advances in Space Research, edited by C. T. Russell, p. 71, Pergamon, Tarrytown, N. Y.

Hoppe, M. M., C. T. Russell, L. A. Frank, T. E. Eastman, and E. W. Greenstadt (1981), Upstream hydromagnetic waves and their association with backstreaming ion populations ISEE 1 and 2 observations, *J. Geophys. Res.*, *86*, 4471–4492.

Jacobsen, K. S., et al. (2009), THEMIS observations of extreme magnetopause motion caused by a hot flow anomaly, *J. Geophys. Res.*, *114*, A08210, doi:10.1029/2008JA013873.

Kajdič, P., X. Blanco-Cano, N. Omidi, and C. T. Russell (2010), Analysis of waves surrounding the foreshock cavitons, *AIP Conf. Proc.*, *1216*, 479–482, doi:10.1063/1.3395907.

Kajdič, P., X. Blanco-Cano, N. Omidi, and C. T. Russell (2011), Multispacecraft study of foreshock cavitons, *Planet. Space Sci.*, *59*, 705–714, doi:10.1016/j.pss.2011.02.005.

Karlsson, T., N. Brenning, H. Nilsson, J.-G. Trotignon, X. Vallières, and G. Facsko (2012), Localized density enhancements in the magnetosheath: Three-dimensional morphology and possible importance for impulsive penetration, *J. Geophys. Res.*, *117*, A03227, doi:10.1029/2011JA017059.

Lacombe, C., and G. Belmont (1995), Waves in the Earth's magnetosheath: Observations and interpretations, in *Physics of Collisionless Shocks*, Advances in Space Research, vol. 15, edited by C. T. Russell, p. 329, Pergamon, Tarrytown, N. Y.

Lacombe, C., F. G. E. Pantellini, D. Hubert, C. C. Harvey, A. Mangeney, G. Belmont, and C. T. Russell (1992), Mirror and Alfvenic waves observed by ISEE 1–2 during crossings of the Earth's bow shock, *Ann. Geophys.*, *10*, 772–784.

Le, G., and C. T. Russell (1992), A study of ULF wave foreshock morphology, II: Spatial variations of ULF waves, *Planet. Space Sci.*, *40*, 1215–1225.

Leroy, M. M., D. Winske, C. C. Goodrich, C. S. Wu, and K. Papadopoulos (1982), The structure of perpendicular bow shocks, *J. Geophys. Res.*, *87*, 5081–5094.
Lin, Y. (1997), Generation of anomalous flows near the bow shock by its interaction with interplanetary discontinuities, *J. Geophys. Res.*, *102*, 24,265–24,281.
Lin, Y. (2002), Global hybrid simulation of hot flow anomalies near the bow shock and in the magnetosheath, *Planet. Space Sci.*, *50*(5–6), 577–591, Symposium on Intercomparative Magetosheath Studies, Antalya, Turkey, Sep 04–08, 2000.
Lin, Y. (2003), Global-scale simulation of foreshock structures at the quasi-parallel bow shock, *J. Geophys. Res.*, *108*(A11), 1390, doi:10.1029/2003JA009991.
Lin, Y., and X. Wang (2005), Three–dimensional global hybrid simulation of dayside dynamics associated with the quasiparallel bow shock, *J. Geophys. Res.*, *110*, A12216, doi:10.1029/2005JA011243.
Lucek, E. A., M. W. Dunlop, A. Balogh, P. Cargill, W. Baumjohann, E. Georgescu, G. Haerendel, and K.-H. Fornacon (1999), Identification of magnetosheath mirror modes in Equator-S magnetic field data, *Ann. Geophys.*, *17*, 1560–1573.
Lucek, E. A., M. W. Dunlop, T. S. Horbury, A. Balogh, P. Brown, P. Cargill, C. Carr, K.-H. Fornaçon, E. Georgescu, and T. Oddy (2001), Cluster magnetic field observations in the magnetosheath: Four-point measurements of mirror structures, *Ann. Geophys.*, *19*, 1421–1428, doi:10.5194/angeo-19-1421-2001.
Lucek, E. A., T. S. Horbury, A. Balogh, I. Dandouras, and H. Rème (2004), Cluster observations of hot flow anomalies, *J. Geophys. Res.*, *109*, A06207, doi:10.1029/2003JA010016.
Luhmann, J. G., C. T. Russell, and R. C. Elphic (1986), Spatial distributions of magnetic field fluctuations in the dayside magnetosheath, *J. Geophys. Res.*, *91*, 1711–1715.
McKean, M. E., D. Winske, and S. P. Gary (1992), Mirror and ion cyclotron anisotropy instabilities in the magnetosheath, *J. Geophys. Res.*, *97*, 19,421–19,432.
McKean, M. E., D. Winske, and S. P. Gary (1994), Two-dimensional simulations of ion anisotropy instabilities in the magnetosheath, *J. Geophys. Res.*, *99*, 11,141–11,153.
Němeček, Z., J. Šafránková, L. Přech, D. G. Sibeck, S. Kokobun, and T. Mukai (1998), Transient flux enhancements in the magnetosheath, *Geophys. Res. Lett.*, *25*, 1273–1276, doi:10.1029/98GL50873.
Omidi, N. (2007), Formation of foreshock cavities, in *Turbulence and Nonlinear Processes in Astrophysical Plasmas*, AIP Conference Proceedings, vol. 932, edited by D. Shaikh and G. Zank, p. 181, AIP, Melville N. Y.
Omidi, N., and D. Sibeck (2007), Formation of hot flow anomalies and solitary shocks, *J. Geophys. Res.*, *112*, A01203, doi:10.1029/2006JA011663.
Omidi, N., A. O'Farrell, and D. Krauss-Varban (1994), Sources of magnetosheath waves and turbulence, *Adv. Space Res.*, *14*(7), 45–54.
Omidi, N., X. Blanco-Cano, C. T. Russell, and H. Karimabadi (2004), Dipolar magnetospheres and their characterization as a function of magnetic moment, *Adv. Space Res.*, *33*(11), 1996–2003.
Omidi, N., X. Blanco-Cano, and C. T. Russell (2005), Macro-structure of collisionless bow shocks: 1. Scale lengths, *J. Geophys. Res.*, *110*, A12212, doi:10.1029/2005JA011169.
Omidi, N., X. Blanco-Cano, C. Russell, and H. Karimabadi (2006), Global hybrid simulations of solar wind interaction with Mercury: Magnetospheric boundaries, *Adv. Space Res.*, *38*, 632–638, doi:10.1016/j.asr.2005.11.019.
Omidi, N., T. Phan, and D. Sibeck (2009a), Hybrid simulations of magnetic reconnection initiated in the magnetosheath, *J. Geophys. Res.*, *114*, A02222, doi:10.1029/2008JA013647.
Omidi, N., D. Sibeck, and X. Blanco-Cano (2009b), The foreshock compressional boundary, *J. Geophys. Res.*, *114*, A08205, doi:10.1029/2008JA013950.
Omidi, N., J. P. Eastwood, and D. G. Sibeck (2010), Foreshock bubbles and their global magnetospheric impacts, *J. Geophys. Res.*, *115*, A06204, doi:10.1029/2009JA014828.
Omidi, N., H. Zhang, D. Sibeck, and D. Turner (2013), Spontaneous hot flow anomalies at quasi-parallel shocks: 2. Hybrid simulations, *J. Geophys. Res. Space Physics*, *118*, 173–180, doi:10.1029/2012JA018099.
Paschmann, G., N. Sckopke, S. J. Bame, J. R. Asbridge, J. T. Gosling, C. T. Russell, and E. W. Greenstadt (1979), Association of low frequency waves with suprathermal ions in the upstream solar wind, *Geophys. Res. Lett.*, *6*, 209–212.
Paschmann, G., G. Haerendel, N. Sckopke, E. Möbius, H. Lühr, and C. W. Carlson (1988), 3-Dimensional plasma structures with anomalous flow directions near the Earth's bow shock, *J. Geophys. Res.*, *93*, 11,279–11,294.
Russell, C. T., and M. Hoppe (1983), Upstream waves and particles, *Space Sci. Rev.*, *34*, 155–172.
Savin, E., et al. (2008), High energy jets in the Earth's magnetosheath: Implications for plasma dynamics and anomalous transport, *JETP Lett.*, *87*(11), 593–599.
Schwartz, S. J. (1995), Hot flow anomalies near the earth's bow shock, in *Physics of Collisionless Shocks*, Advances in Space Research, edited by C. T. Russell, p. 107, Pergamon, Tarrytown, N. Y.
Schwartz, S. J., R. L. Kessel, C. C. Brown, L. J. C. Woolliscroft, M. W. Dunlop, C. J. Farrugia, and D. S. Hall (1988), An active current sheet near the earth's bow shock, *J. Geophys. Res.*, *93*, 11,295–11,310.
Schwartz, S. J., G. Paschmann, N. Sckopke, T. M. Bauer, M. Dunlop, A. N. Fazakerley, and M. F. Thomsen (2000), Conditions for the formation of hot flow anomalies, *J. Geophys. Res.*, *105*, 12,639–12,650.
Sckopke, N., G. Paschmann, S. J. Bame, J. T. Gosling, and C. T. Russell (1983), Evolution of ion distributions across the nearly perpendicular bow shock: Specularly and non-specularly reflected ions, *J. Geophys. Res.*, *88*, 6121–6136.
Sckopke, N., G. Paschmann, A. L. Brinca, C. W. Carlson, and H. Lühr (1990), Ion thermalization in quasi-perpendicular shocks involving reflected ions, *J. Geophys. Res.*, *95*, 6337–6352.
Seon, J., S. M. Park, K. W. Min, L. A. Frank, W. R. Paterson, and K. W. Ogilvie (1999), Observations of density fluctuations in Earth's magnetosheath with Geotail and Wind spacecraft, *Geophys. Res. Lett.*, *26*, 959–962, doi:10.1029/1999GL900131.
Sibeck, D. G., and J. T. Gosling (1996), Magnetosheath density fluctuations and magnetopause motion, *J. Geophys. Res.*, *101*, 31–40, doi:10.1029/95JA03141.
Sibeck, D. G., et al. (1999), Comprehensive study of the magnetospheric response to a hot ow anomaly, *J. Geophys. Res.*, *104*, 4577–4593.
Sibeck, D. G., et al. (2000), Magnetopause motion driven by interplanetary magnetic field variations, *J. Geophys. Res.*, *105*, 25,155–25,169.
Sibeck, D. G., N. Omidi, I. Dandouras, and E. Lucek (2008), On the edge of the foreshock: Model-data comparisons, *Ann. Geophys.*, *26*, 1539–1544.
Sibeck, D., N. Borodkova, G. Zastenker, S. Romanov, and J. Sauvaud (1998), Gross deformation of the dayside magnetopause, *Geophys. Res. Lett.*, *25*, 453–456.
Thomas, V., D. Winske, M. F. Thomsen, and T. G. Onsager (1991), Hybrid simulation of the formation of a hot flow anomaly, *J. Geophys. Res.*, *96*, 11,625–11,632.

Thomsen, M. F., J. T. Gosling, S. A. Fuselier, S. J. Bame, and C. T. Russell (1986), Hot diamagnetic cavities upstream of the earth's bow shock, *J. Geophys. Res.*, *91*, 2961–2973.

Thomsen, M. F., J. T. Gosling, S. J. Bame, K. B. Quest, C. T. Russell, and S. A. Fuselier (1988), On the origin of hot diamagnetic cavities near the earth's bow shock, *J. Geophys. Res.*, *93*, 11,311–11,325.

Thomsen, M. F., V. A. Thomas, D. Winske, J. T. Gosling, M. H. Farris, and C. T. Russell (1993), Observational test of hot flow anomaly formation by the interaction of a magnetic discontinuity with the bow shock, *J. Geophys. Res.*, *98*, 15,319–15,330.

Turner, D. L., S. Eriksson, T. D. Phan, V. Angelopoulos, W. Tu, W. Liu, X. Li, W.-L. The, J. P. McFadden, and K.-H. Glassmeier (2011), Multispacecraft observations of a foreshock-induced magnetopause disturbance exhibiting distinct plasma flows and an intense density compression, *J. Geophys. Res.*, *116*, A04230, doi:10.1029/2010JA015668.

Turner, D. L., N. Omidi, D. G. Sibeck, and V. Angelopoulos (2013), First observations of foreshock bubbles upstream of Earth's bow shock: Characteristics and comparisons to HFAs, *J. Geophys. Res. Space Physics*, *118*, 1552–1570, doi:10.1002/jgra.50198.

Zastenker, G. N., M. N. Nozdrachev, Z. Nemecek, J. Safrankova, K. I. Paularena, J. D. Richardson, R. P. Lepping, and T. Mukai (2002), Multispacecraft measurements of plasma and magnetic field variations in the magnetosheath: Comparison with Spreiter models and motion of the structures, *Planet. Space Sci.*, *50*, 601–612, doi:10.1016/S0032-0633(02)00039-9.

Zhang, H., D. G. Sibeck, Q.-G. Zong, N. Omidi, D. Turner, and L. B. N. Clausen (2013), Spontaneous hot flow anomalies at quasi-parallel shocks: 1. Observations, *J. Geophys. Res. Space Physics*, *118*, 3357–3363, doi:10.1002/jgra.50376.